Evaluating the corrosion and wear behaviour of high velocity oxygen fuel sprayed titanium iron oxide modified with nickel-chromium coating on plain carbon steel

by M. Raoufi[1], Y. Naami[1], Z.M. Beiranvand[1], M. Moghaddasi[2], A. Naeimi[3]

Affiliation:
[1] Department of Materials Science and Engineering, Faculty of Engineering, Arak University, Iran
[2] Corrosion and Coating Inspection Department, Imam Khomeini Oil Refinery Company, Iran
[3] Department of Mechanical and Energy Systems Engineering / Energy Systems Engineering, Shahid Beheshti University, Iran

Correspondence to:
M. Raoufi

Email:
m-raoufi@araku.ac.ir

Dates:
Received: 31 May 2024
Revised: 7 Jul. 2025
Accepted: 01 Oct. 2025
Published: May. 2026

How to cite:
Raoufi, M., Naami, Y., Beiranvand, Z.M., Moghaddasi, M., Naeimi, A. 2026. Evaluating the corrosion and wear behaviour of high velocity oxygen fuel sprayed titanium iron oxide modified with nickel-chromium coating on plain carbon steel. *Journal of the Southern African Institute of Mining and Metallurgy*, vol. 126, no. 5, pp. 253 - 260

DOI ID:
https://doi.org/10.17159/2411-9717/3242/2026

ORCiD:
M. Raoufi
https://orcid.org/0000-0001-8487-8934
Z.M. Beiranvand
https://orcid.org/0009-0009-1945-4954
A. Naeimi
https://orcid.org/0000-0003-2408-7844

Abstract

Titanium iron oxide and nickel-chromium coatings were applied on low-carbon steel substrates using the high-velocity oxygen fuel thermal spraying process. The microstructure, phase composition, and hardness of the coatings were analysed using scanning electron microscopy, x-ray diffraction, and microhardness tests. The phase analysis confirmed the formation of oxide compounds in the coatings. The average microhardness values for titanium iron oxide and titanium iron oxide-nickel-chromium coatings were measured at 580 HV and 970 HV, respectively, under a 100 g load. The corrosion resistance of the coatings was evaluated in a 3.5% sodium chloride solution using electrochemical impedance spectroscopy (EIS) and polarisation tests. The results indicated that the nickel-chromium composition exhibited superior corrosion resistance, which was attributed to its low porosity, preventing solution diffusion into the substrate. Wear behaviour was assessed using a pin-on-disk test with a tungsten carbide pin as the counterbody. The incorporation of nickel-chromium into the titanium iron oxide coating resulted in an 80% reduction in weight loss, indicating significant improvement in wear resistance. These findings suggest that nickel-chromium-modified titanium iron oxide coatings enhance both corrosion and wear resistance, making them promising candidates for industrial applications.

Keywords
coating, high velocity oxygen fuel VOF, nickel-chromium, corrosion, wear, titanium iron oxide

Introduction

Carbon steel is among the most extensively utilised engineering alloys, particularly in the automobile, oil and gas, and petrochemical industries. Despite its widespread use, the surface of plain carbon steel is highly susceptible to degradation mechanisms such as wear, oxidation, and corrosion (Sidhu et al., 2007; Galedari et al., 2019; Ding et al., 2018; Torbati-Sarraf, Poursaee, 2018). The surface condition of metals plays a critical role across various industries, as it directly influences the performance and durability of components. To address these demands, the development of advanced surface engineering processes and technologies has become essential to enhance the quality, longevity, and operational efficiency of components. Surface coating techniques are widely employed to improve the surface properties and extend the service life of carbon steel components. Among these techniques, thermal spraying has gained significant attention. It encompasses a variety of processes used to apply both metallic and non-metallic coatings for improved surface performance (Tobergte, Curtis, 2013). High velocity oxygen fuel (HVOF) spraying is a prominent thermal spraying technique known for producing dense and well-adhered coatings. It is extensively used for coating industrial components in sectors such as oil and gas, aerospace, and agriculture, primarily to enhance surface resistance against corrosion and wear (Sidhu et al., 2007; Jones et al., 2001; Singh et al., 2019; Yilbas et al., 2003; Park et al., 2013). Thermal spraying involves the deposition of molten or semi-molten particles onto a substrate surface to form a coating, offering advantages such as process simplicity and cost-effectiveness (Wei et al., 2023; Hong et al., 2023). Among the various thermal spraying techniques, coatings produced by HVOF method are particularly notable for their high density, low porosity, elevated hardness, and strong adhesion to the substrate (Zhao, Lugscheider, 2003; Lekatou et al., 2008; Hong et al., 2014; Xie et al., 2013). As a result, HVOF is widely employed to extend the service life span of components and improve manufacturing efficiency across a range of materials. Furthermore, HVOF-deposited cermet coatings have been developed with excellent bonding characteristics and superior resistance to wear and corrosion, thereby optimising in-service performance in demanding industrial applications (Stokes, Looney, 2004; Li et al., 1996; Karimi et al., 1995). Various coatings have been developed using thermal spraying techniques to enhance wear and corrosion resistance. Verdian et al. (2010; 2012) reported favorable corrosion resistance in coatings such as nickel titanium (NiTi) and nickel silicide composites or commonly known as niobium (Ni (Si)/Ni_5Si) produced via thermal spraying. These coatings exhibited high hardness and strong bond strength, outperforming the substrate when immersed in a 3.5% sodium chloride (NaCl) corrosion solution. The incorporation of nickel in the coatings contributed significantly to corrosion resistance, primarily due to the reduced oxidation during the spraying process. Furthermore, the addition of hard particles such as chromium improved the coatings' wear resistance by forming a more robust structure (Verdian et al., 2012; Ak et al., 2003; Zavareh et al., 2016; Karaoglanli et al., 2017). Nickel and cobalt are among the most suitable materials for coatings applied via the HVOF method, as they tend to produce dense coatings with low porosity and have demonstrated effectiveness as barriers against electrolyte permeation. Consequently, exploring coatings based on other metals—particularly nickel and cobalt—as alternatives to niobium for protection against hydrogen embrittlement and as hydrogen barriers, using HVOF thermal spray techniques, is both promising and of significant practical relevance (Brandolt et al., 2019). In a study conducted by Brandolt et al. (2019), micro-printing techniques were employed on thermally sprayed coatings to investigate the mechanisms of hydrogen trapping within the coating layers. Oxide coatings are widely employed across various industries due to their excellent protective properties. However, to date, titanium iron oxide powder has not been extensively utilised as a coating material. Oxide coatings are particularly attractive in surface engineering due to their excellent chemical stability, high-temperature resistance, and ability to form dense, adherent layers that act as effective barriers against corrosive agents. These coatings can significantly reduce oxidation and material degradation in harsh environments, making them suitable for demanding industrial applications. Additionally, their inherent hardness and wear resistance contribute to improved mechanical durability, which is essential for extending the service life of components exposed to friction, erosion, or corrosive media (Sidhu, Prakash, 2006). In this study, titanium iron oxide is applied in combination with nickel and chromium (NiCr) using HVOF thermal spraying process. During solidification from high temperatures, the conditions facilitate the formation of oxides within the coating structure. This results in the development of a continuous and stable oxide layer that serves as an effective protective barrier. The oxide layer acts as a dense shield, preventing the penetration of oxygen and corrosive agents to the steel surface, while also enhancing resistance to scratching and friction. Consequently, surface degradation of the substrate is significantly reduced. The primary objective of this research is to investigate the corrosion and wear behavior of titanium iron oxide-NiCr and titanium iron oxide coatings deposited via the HVOF process. It is anticipated that this composition of powder will enhance both corrosion and wear resistance of industrial components, owing to the presence of elements with high resistance to oxidation and mechanical wear—ultimately contributing to extended service lifespan of the substrate.

Materials and methods

The material used in this research work was titanium iron oxide together with NiCr. This powder was produced from an inorganic mineral that was subjected to a milling process for 8 hours in order to be finer. Then, about 70% of titanium iron oxide powder was mixed into the mill with 30% of NiCr powder for 4 hours. The rotation speed of the container in the milling process was considered about 180 rpm. The milling powders with a size of 15 μm – 45 μm were implemented for use in the spraying process. The coating was applied on the substrate of low-carbon steel having the dimensions of 20*20*80 mm^3. At first, the surface of the samples was cleaned and uniformed by a stonemason device-equipped magnetic table. Then, before applying the coating, sandblasting was executed by means of alumina powder with mesh 20 to create appropriate roughness on the surface. Finally, the samples were degreased by rinsing it with acetone solution. The MJ5000 model thermal spraying with 8-axis robotic system was utilised to create titanium iron oxide and titanium iron oxide-NiCr coatings. The coating improvement parameters are presented in Table 1.

Table 1

HVOF process parameters

Gas flow	Carrier gas pressure (kPa)	Particle size (μm)	Spray distance (cm)	Fuel flow (ml/min)
N2	600	15-45	30	380

X-ray diffraction (XRD) was used by ASENWARE device (model AW-XDM300) under 40 KV voltage and 30 mA current to investigate the exist phases in the obtained compacted powders and coatings. Finally, phase matching was performed by Xpert high Score software. Scanning electron microscopy (SEM) (model LE1455VP) was utilised to observe the microstructure and measure the thickness of the coatings. For that purpose, several cross-sections were provided from the coated samples. These cross-sections were grinded. Before sanding, mounts were used to avoid detaching the coating as well as proper sanding of the sample edges. The hardness test was performed by Vickers micro-hardness device under operating conditions of 100 g applying load and 15 s time with 3 iterations. Scanning electron microscopy was used to investigate the porosity of the coatings. After comparing the micrographs with each other and identifying the porosities, their amount was determined by Image J software. The corrosion test of steel samples with a coating was done in a 3.5% NaCl solution. Before commencing the experiment, to reach the surface reaction of the samples with the electrolyte solution, the open circuit potential of each sample was monitored for 30 min. The Tafel polarisation test was carried out by Autolab Potentiostat device (model PG STAT302N), which was attached to a three-electrode cell composing of the sample, reference saturated calomel electrode, and platinum auxiliary electrode. This test was accomplished in the range of -0.5 V to +1 V in comparison with the open circuit having a corrosion rate of 2 mVs^{-1}. Electrochemical impedance spectroscopy (EIS) was implemented in the frequency range of 10 kHz to 100 mHz in the open circuit potential. In order to study the results of this test, Nova1.8 software was used. The pin-on-disk test was executed to determine the wear resistance and friction coefficient of the coatings. This test was evaluated using a tungsten carbide (WC) pin with 75 RC hardness under a 10 N applied force over the distance of 1000 m. After completion of the test, to completely discard the eroded particles adhered to the surface, the sample was rinsed. At that time, the eroded surface of the coating was evaluated to investigate the wear mechanism of the coatings using SEM.

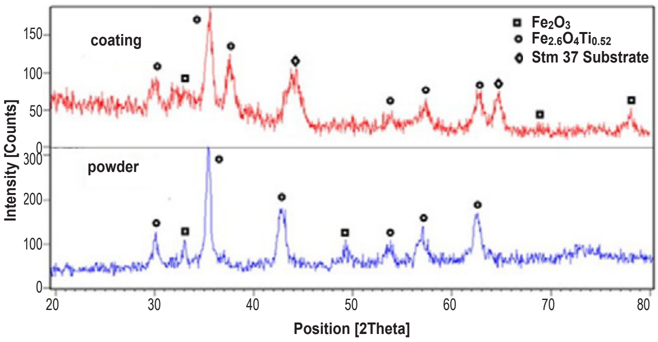

Figure 1—XRD patterns of titanium iron oxide powder and HVOF titanium iron oxide coating

Results and discussion

X-ray diffusion pattern

X-ray diffusion (XRD) patterns of the titanium iron oxide powder and the deposited coating are presented in Figure 1. The XRD analysis reveals that the primary phases present in the ground powder include Fe_3O_4 (magnetite) and $Fe_{2.6}Ti_{0.56}O_4$, which are consistent with previously reported compositions in similar oxide systems. As shown in Figure 1, these phases are also observed at similar diffraction angles in the coating produced via the thermal spraying process, indicating that the phase composition is largely retained during deposition. In addition, diffraction peaks corresponding to the St37 steel substrate are also detectable, suggesting partial penetration or exposure of the substrate during analysis.

Figure 2 presents the XRD patterns of the crushed mineral powder after the addition of NiCr, along with the corresponding coating produced from this composite powder. The results indicate that the mechanical milling of titanium iron oxide with NiCr led to the formation of several new phases. In addition to the phases identified in the previous coating, new peaks corresponding to $FeNi_3$, metallic nickel (Ni), and metallic chromium (Cr) are observed in the diffraction pattern. These findings suggest that the incorporation of NiCr significantly alters the phase composition of the coating, likely enhancing its structural and functional properties.

A comparison between the XRD patterns of the powder and the corresponding coating after thermal spraying reveals a broadening of the diffraction peaks and a reduction in their intensity. According to previous studies (Verdian et al., 2010; Verdian et al., 2012), this phenomenon can be attributed to the high kinetic energy of the semi-molten particles during the HVOF spraying process.

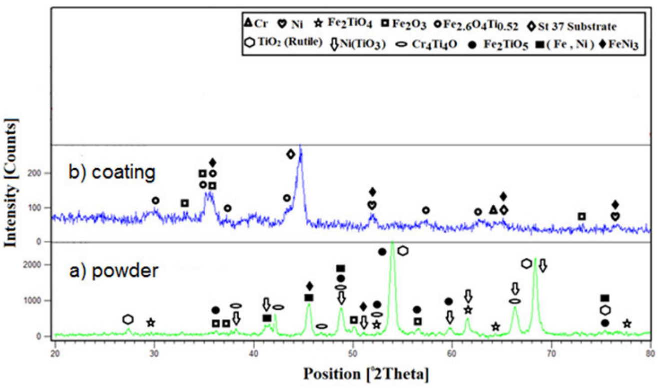

Figure 2—XRD patterns of (a) titanium iron oxide -NiCr powder and (b) HVOF titanium iron oxide -NiCr coating

Upon impact with the underlying surface, these particles undergo severe plastic deformation, which leads to grain refinement and an increase in internal strain energy—both of which contribute to peak broadening and intensity reduction in the diffraction pattern.

Scanning electron microscopy images

Figure 3 shows scanning electron microscopy (SEM) images of the coating surfaces produced by the HVOF thermal spraying process. In this method, particles are deposited in molten or semi-molten states due to the relatively low internal heat input, which contributes to coatings with minimal defects (Puetz et al., 2010). The SEM image of the titanium iron oxide coating in Figure 3(a) reveals a small number of pores and craters and no visible cracks. This may be attributed to the difference in melting points between Fe_2O_3 and TiO_2, which results in the formation of more spherical features on the coating surface. Additionally, due to the proximity between the melting point of Fe and the temperatures reached during HVOF spraying, Fe and Ti particles may remain unmelted or only partially melted during deposition. As shown in Figure 3(b), the number of pores and craters decreases with the incorporation of NiCr into the titanium iron oxide powder, suggesting that Ni and Cr fill the voids within the coating structure. All coatings exhibit a uniform, homogeneous surface with minimal oxidation and no surface cracks, indicating good coating quality across all systems.

Figure 4 presents cross-sectional SEM images of the coatings produced via the HVOF thermal spraying method. All micrographs clearly show good adhesion between the coating and the substrate, with no visible signs of delamination or interfacial separation (Sadeghimeresht et al., 2017; Brito et al., 2012). As observed in Figure 4a, the titanium iron oxide coating exhibits notable porosity, cracks, and a distinct dark oxide layer. According to energy dispersive spectroscopy (EDS) analysis, this oxide-rich layer contains a high proportion of iron (Fe: 81.83 wt%, Ti: 8.94 wt%, O: 9.23 wt%). Iron remains the dominant element throughout the titanium iron oxide coating; however, its concentration significantly decreases upon the addition of NiCr (Fe: 37.80 wt%, Ti: 4.09 wt%,

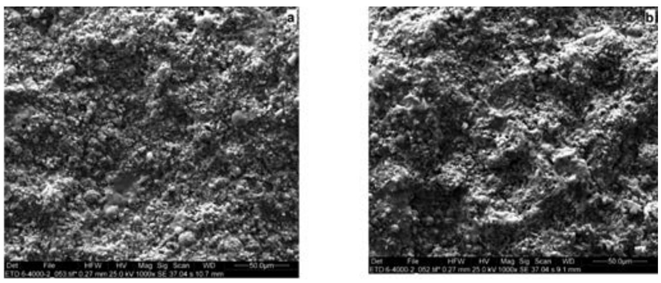

Figure 3—Surface SEM images of coatings (a) titanium iron oxide, (b) titanium iron oxide -NiCr

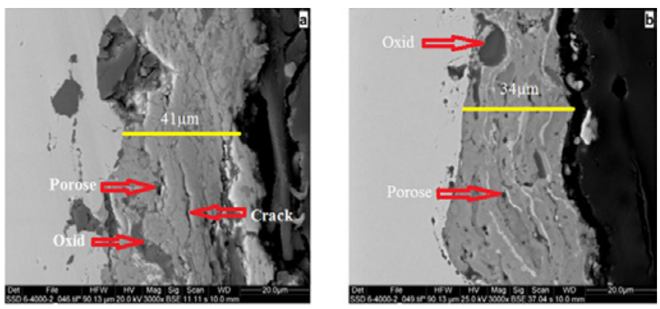

Figure 4—Cross-sectional SEM images of coatings: (a) Fe_3TiO_4, (b) Fe_3TiO_4-NiCr

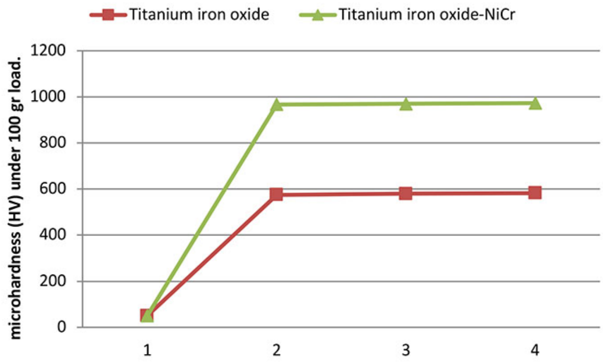

Figure 5—The average microhardness values of the HVOF coatings

O: 6.19 wt%, Cr: 43.88 wt%, Ni: 2.39 wt%). The average thickness and porosity of the titanium iron oxide and titanium iron oxide-NiCr coatings were measured as 41 µm with 1.3% porosity, and 34 µm with 0.4% porosity, respectively. These results indicate effective integration of Ni and Cr particles with the titanium iron oxide matrix. During the spraying process, NiCr particles appeared to have completely melted and, upon impact with the substrate, infiltrated the underlying layers, effectively filling voids and reducing overall porosity. Consequently, the titanium iron oxide-NiCr coating exhibits a denser microstructure and thinner layer compared to the titanium iron oxide-only coating. The low porosity and high density observed in both coatings are attributed to the high-velocity impact of particles during HVOF spraying, which enhances packing efficiency and reduces the presence of voids and defects.

In conclusion, the thermal spraying process using the HVOF technique successfully produced coatings with high density and excellent adhesion to the substrate—key advantages of this method (Suarez et al., 2008; Murthy, Venkataraman, 2006). The incorporation of NiCr significantly reduced the size and volume of porosities within the coating, indicating a denser microstructure in the titanium iron oxide-NiCr coating compared to titanium iron oxide alone. Since porosity plays a critical role in determining the corrosion performance of coatings, this reduction is especially beneficial. The presence of fewer and smaller pores in the structure enhances the barrier properties of the coating, thereby improving its corrosion resistance (Zhao et al., 2005).

Hardness measurements

Figure 5 presents the measured average microhardness values of the titanium iron oxide and titanium iron oxide-NiCr coatings. A significant difference in hardness between the two coatings is evident. This variation can be attributed to several factors, including porosity levels, the proportion of unmelted and semi-melted particles, the presence of fully melted and rapidly solidified particles, oxide phases, and differences in grain size and morphology—all of which are known to influence the hardness of thermally sprayed coatings (Mahesh et al., 2008; Kamal et al., 2010). The reduced porosity observed in the titanium iron oxide-NiCr coating, due to the incorporation of hard NiCr particles, contributes to the increase in hardness. Moreover, the XRD analysis confirms the presence of hard phases such as TiO_2, Fe_2O_3, Cr, and Ni in the NiCr-containing coating, further enhancing its hardness. Notably, the addition of 30 wt% NiCr to the titanium iron oxide powder resulted in a substantial improvement in hardness, suggesting that this composition may represent an optimal reinforcement level for maximising hardness performance.

Polarisation results

Figure 6 illustrates the Tafel polarisation curves of the coatings produced via the HVOF thermal spraying process, along with the uncoated steel substrate, in a 3.5% NaCl solution under ambient conditions.

The extracted electrochemical parameters of these curves, such as corrosion potential (E_{corr}), corrosion flow density (i_{corr}) (corrosion rate) cathodic and anodic Tafel slips, which were obtained using the Tafel extrapolation method, are presented in Table 2. Based on Table 2, the coating containing NiCr exhibits a more noble corrosion potential compared to both the substrate and the NiCr-free coating, indicating improved corrosion resistance.

The corrosion, current density significantly decreases with the addition of NiCr particles, and the corrosion potential shifts toward more positive values. As observed in the Tafel curve, the coated samples exhibit a passive-like behaviour. The corrosion rate of the uncoated sample is 112 µAcm^{-2}, while the sample with the titanium iron oxide coating shows a corrosion rate of 315 µAcm^{-2}, which leads to the breakdown of the passive-like layer at higher anodic

Table 2

Corrosion parameters estimated from the polarization cures

	E_{corr} (mV)	i_{corr} (µAcm^{-2})	β_a (mV-dec^{-1})	β_c (mV-dec-1)
St37	-633	112	108	82
Titanium iron oxide	-509	315	179	161
Titanium iron oxide-NiCr	-488	42	86	43

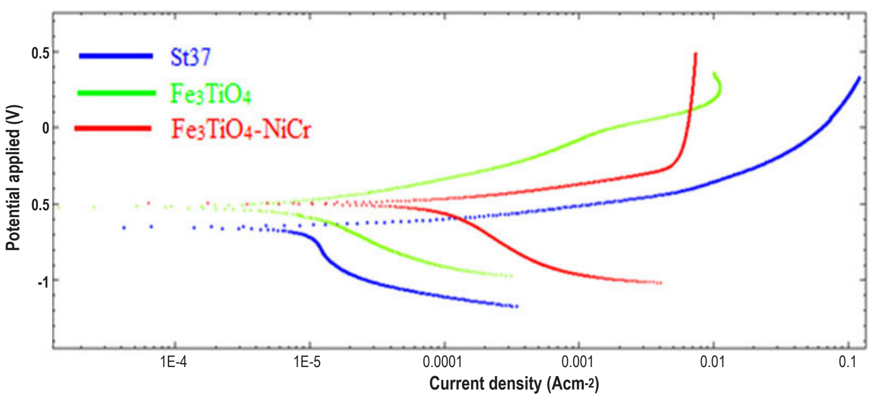

Figure 6—Polarisation curves of St37 steel substrate, HVOF titanium iron oxide (Fe_3TiO_4) and titanium iron oxide-NiCr coatings in 3.5% NaCl solution

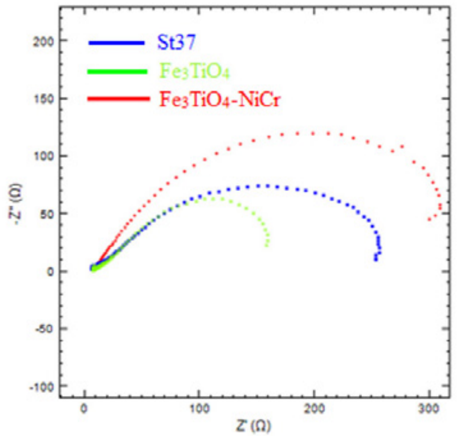

Figure 7—Experimental Nyquist diagram for steel substrate and HVOF coatings in 3.5% NaCl solution

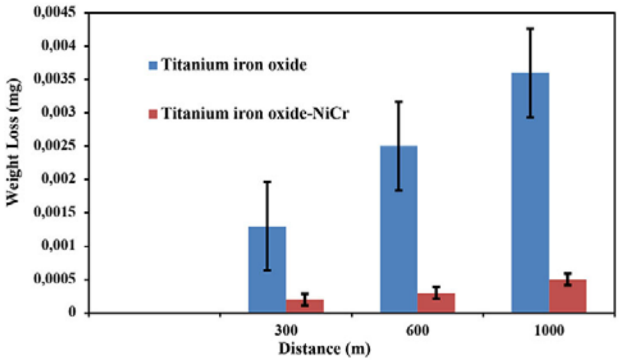

Figure 8—Wear rate of coatings

potentials around -0.1 V. Notably, the corrosion rate is reduced to 42 μAcm^{-2} with the addition of NiCr. This reduction can be attributed to the passive-like behaviour of the NiCr coating at high anodic potentials, which prevents electrolyte diffusion into the underlying layers, resulting in a decrease in the corrosion current density and enhanced stability at higher potentials. In other words, the passive-like layer in the NiCr coating is not porous. Therefore, it causes disruption of the electron transfer on the surface and obstructs it from participating in electrochemical reactions. This behaviour has a high resistance in comparison with other researchers (Verdian et al., 2010; Myalska et al., 2017; Pileggi et al., 2015; Hassannejad et al., 2017). The Nyquist plot for the coated samples and the steel substrate is shown in Figure 7.

In this circuit, a capacitive ring is observed, which is associated with the coating resistance on the electrode surface. The impedance data extracted from the equivalent circuit include charge transfer resistance (Rct), a constant phase element (Q) representing the capacitor behaviour, and the Ohmic resistance of the electrolyte, which remains low across all samples (11.2 $\Omega{\cdot}cm^2$ – 13.5 $\Omega{\cdot}cm^2$). As shown in Figure 7, the titanium iron oxide coating exhibits the smallest diameter of the semicircle, indicating a relatively low charge transfer resistance (167 $\Omega{\cdot}cm^2$), compared to the steel substrate (270 $\Omega{\cdot}cm^2$). The charge transfer resistance is directly related to electron transfer across the coating surface and inversely proportional to the corrosion rate. The charge transfer resistance increases with the addition of NiCr to the titanium iron oxide coating (312 $\Omega{\cdot}cm^2$), which corresponds to the largest diameter of the semicircle. The enhancement in charge transfer resistance in the titanium iron oxide-NiCr coating is attributed to the high resistance of the dual-layer structure against the penetration of corrosive agents into the underlying layers, which is facilitated by the uniform distribution of nickel and chromium particles on the coating surface and between the layers. The high correlation between the experimental data and the proposed equivalent circuit further demonstrates the accuracy of the model used to describe the corrosion behaviour of the samples in a corrosive environment. This behaviour is similar to that observed in other dense coatings, such as stainless-steel coatings, TiNi coatings with TiO_2 particles, and WC-CoCr coatings, which exhibit passive behaviour (Magnani et al., 2007; Cheng et al., 2004; Guilemany et al., 2006).

Wear results

Figure 8 presents the weight loss data of the titanium iron oxide and titanium iron oxide-NiCr coating samples after undergoing a continuous 1000-metre sliding distance. The results show that the weight loss for the titanium iron oxide sample is 0.0036 g, while the weight loss significantly decreases to 0.0005 g upon adding NiCr particles, forming the titanium iron oxide-NiCr coating. This reduction in weight loss for the titanium iron oxide-NiCr coating is attributed to its higher hardness, which results in a lower wear rate compared to the titanium iron oxide coating. This trend aligns with Archard's wear law (Zmitrowicz, 2006), which is expressed as:

$$Q = K\frac{W}{H} \quad [1]$$

Where Q denotes the wear volume in the slipway unit, W is the applying load, H is the hardness and K defines as the wear coefficient. Hence, weight loss of the coating during the wear test has a reverse relation with its hardness. The results of several researchers show the correctness of this issue (Fang et al., 2009; Lih et al., 2000). Many research studies have been conducted on the effect of NiCr on the wear resistance. Their results indicate that the wear rate is lessened by adding NiCr particles and led to the improvement of the wear resistance (Zavareh et al., 2016; Karaoglanli et al., 2017).

Figure 9 presents the variation of the friction coefficient for the HVOF-coated samples. The curves exhibit significant fluctuations, which are attributed to the repeated adhesion and detachment of wear particles. These fluctuations lead to periodic increases and decrease in the force exerted between the abrasive and the coating surface. At the beginning of the test, the friction coefficient for the titanium iron oxide-NiCr coating is notably lower than that of the titanium iron oxide coating. The high slope observed at the start of the friction coefficient curve for the titanium iron oxide coating can be explained by the rapid accumulation of wear particles. These particles accumulate between the two contacting surfaces, which increases the wear rate. As the test progresses, the removal of some particles results in a reduction in the friction coefficient. The stability of the friction curve for titanium iron oxide occurs when the number of particles generated and trapped between the surfaces is balanced by the number of particles removed from the surfaces.

The coating containing NiCr exhibits lower roughness compared to the titanium iron oxide coating. According to the findings of Magnani et al. (2004), coatings with lower roughness are expected to stabilise more quickly or over shorter distances. However, in this study, the titanium iron oxide-NiCr coating behaves contrary to these expectations. This discrepancy can be attributed to the increased temperature at the contact point of the abrasive particles, caused by the frictional heat. This elevated temperature leads to the oxidation of the particles (Magnani et al., 2008; Srinivasan et al., 2012). The images in Figure 10 (a) and (c) show SEM micrographs of the worn paths of the titanium iron oxide and titanium iron oxide-NiCr coatings at 200 x magnification.

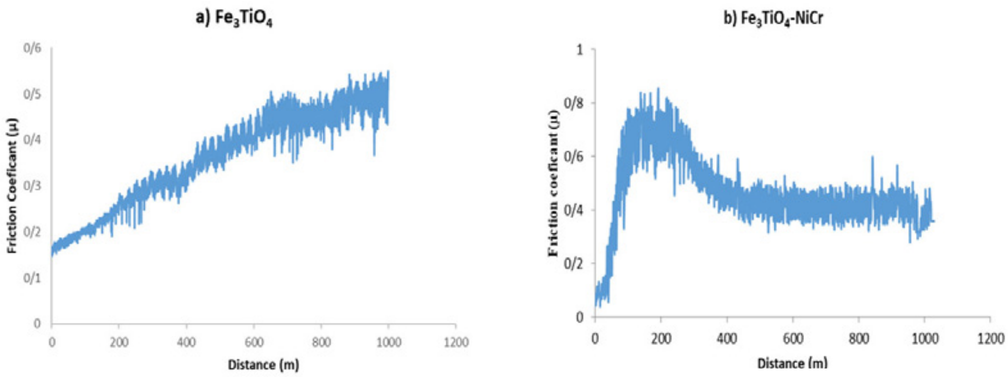

Figure 9—Evolution of the friction for HVOF (a) Fe_3TiO_4, and (b) Fe_3TiO_4-NiCr coatings

The wear on the NiCr-containing coating is negligible compared to the titanium iron oxide coating, owing to the lower roughness and the presence of hard phases. No signs of lamination (ductility) or particle breakage were observed in either coating. Only micro-scratches, indicative of abrasion, were visible, aligned in the direction of the wear. These grooves suggest a shredding mechanism. In higher magnification images (Figure 10b and 10d), white areas are visible, which likely indicate particle detachment, pointing to an adhesion mechanism in operation. SEM images of both coatings show no microcracks, delamination, or any destructive effects. Furthermore, due to the higher hardness and lower friction coefficient of the titanium iron oxide-NiCr coating, the wear tracks appear smoother and less pronounced, as seen in the microscopic images of this coating (Karaoglanli et al., 2017).

Conclusion

The HVOF technique has been used to deposit titanium iron oxide and titanium iron oxide-NiCr coatings on St37 carbon steel substrate and the micro-structure; corrosion resistance and wear resistance were characterised. The following observations were made based on the present study.

- The porosity amount of the coating was decreased from 1.4% in the sample without NiCr to 0.4 % in the sample with NiCr, which indicates a coating with high density and hardness and strong bond strength.
- The coating hardness was increased from 570 HV to 970 HV by adding NiCr.
- The incorporation of NiCr into the titanium iron oxide coating led to a significant improvement in corrosion resistance, as indicated by the decrease in corrosion current density (i_{corr}) from 315 μAcm^{-2} for the titanium iron oxide coating to 42 μAcm^{-2} for the titanium iron oxide-NiCr coating, and a positive shift in corrosion potential (E_{corr}) from -509 mV to -488 mV. These results demonstrate the formation of a more stable and protective passive-like layer, effectively enhancing the corrosion resistance of the coating.

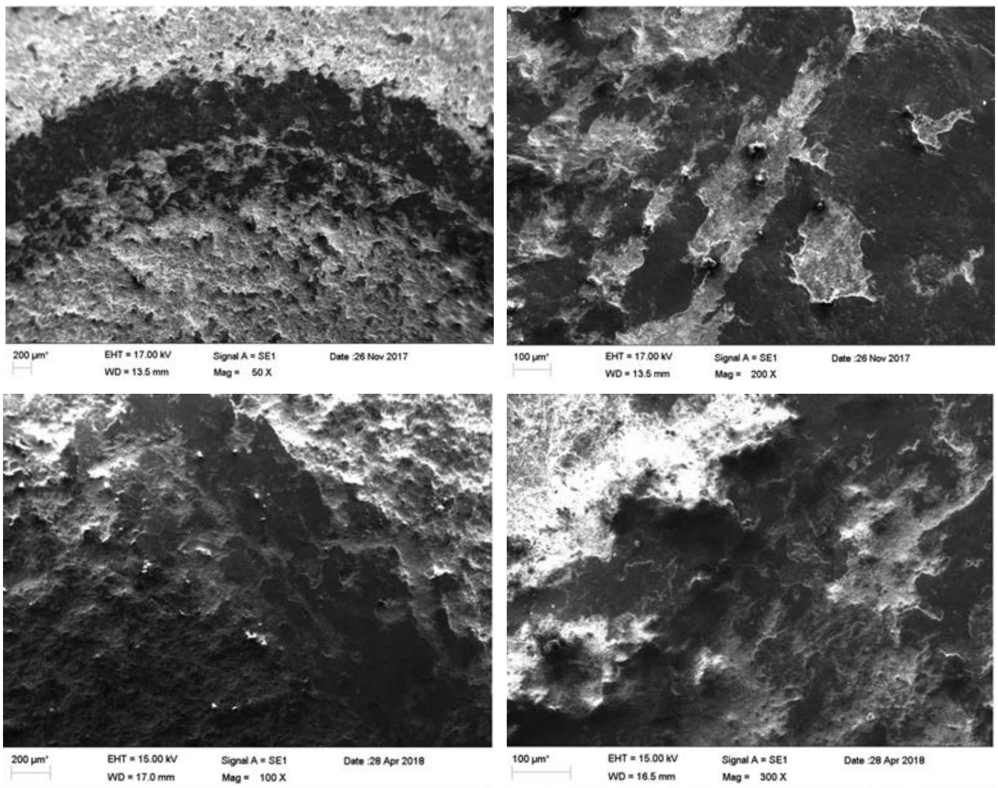

Figure 10—SEM images of wear tracks on (a, b) titanium iron oxide and (c, d) titanium iron oxide-NiCr coatings

- The weight loss of the titanium iron oxide-NiCr coating was low due to the presence of the NiCr particles. Besides, the wear behaviour was improved owing to the formation of the hard phases.

References

Ak, N.F., Tekmen, C., Ozdemir, I., Soykan, H.S., Celik, E. 2003. NiCr Coatings on Stainless Steel by HVOF Technique, *Surfcoat Coatings Technology*, 174–175, p 1070–1073. doi:10.1016/S0257-8972(03)00367-0

Brandolt, C.S., Malfatti, C.F., Ortega Vega, M.R., Navarro Hidalgo, G.E., R. M. Schroeder, R.M. 2019. Determination of hydrogen trapping mechanisms by microprinting in Ni and Co coatings obtained by HVOF. *Surface and Coatings Technology*, vol. 362, pp. 262–273. doi.org/10.1016/j.surfcoat.2019.01.111

Cheng, F., Shi, P., Man, H. 2004. A Preliminary Study of TiO_2 Deposition on NiTi by a Hydrothermal Method. *Surfcoat Coatings Technology,* vol. 187, no. 1, p 26–32. doi:10.1016/j.surfcoat.2004.01.023

Ding, L., Torbati-Sarraf, H., Poursaee, A. 2018. The Influence of the Sandblasting as a Surface Mechanical Attrition Treatment on the Electrochemical Behavior of Carbon Steel in Different PH Solutions. *Surfcoat Coatings Technology*, vol. 352, pp. 112–119.

Fang, W., Cho, T.Y., Yoon, J.H., Song, K.O., Hur, S.K., Youn, S.J., Chun, H.G. 2009. Processing Optimization, Surface Properties and Wear Behavior of HVOF Spraying WC–CrC–Ni Coating. *Journal of Material Processing Technology*, vol. 209, no. 7, pp. 3561–3567. doi:10.1016/j.jmatprotec.2008.08.024

Galedari, S.A., Mahdavi, A., Azarmi, F., Huang, Y., McDonald, A. 2019. A Comprehensive Review of Corrosion Resistance of Thermally-Sprayed and Thermally-Diffused Protective Coatings on Steel Structures. *Journal of Thermal Spray Technology*, vol. 8, no. 4, p 645–677. doi:10.1007/s11666-019-00855-3

Guilemany, J.M., Fernández, J., Espallargas, N., Suegama, P.H., Benedetti, A.V. 2006. Influence of Spraying Parameters on the Electrochemical Behaviour of HVOF Thermally Sprayed Stainless Steel Coatings in 3.4% NaCl. *Surfcoat Coatings Technology*, 2006, vol. 200, no. 9, p 3064–3072. doi:10.1016/j.surfcoat.2005.02.116

Hassannejad, H., Moghaddasi, M., Saebnoori, E., Baboukani, A.R. 2017. Microstructure, Deposition Mechanism and Corrosion Behavior of Nanostructured Cerium Oxide Conversion Coating Modified with Chitosan on AA2024 Aluminum Alloy. *Journal of Alloys and Compounds*, vol. 725, p 968–975. doi:10.1016/j.jallcom.2017.07.253

Hong, S., Wu, Y.P., Gao, W.W., Wang, B., Guo, W.M., Lin, J.R. 2014. Microstructural Characterisation and Microhardness Distribution of HVOF Sprayed WC–10Co–4Cr Coating. *Surfcoat Eng*, vol. 30, no. 1, pp. 53–58. doi:10.1179/1743294413Y.0000000184

Hong, S., Wang, Z., Lin, J.R., Cheny, J.B., Sun, W., Y. Zheng, Y. 2023. Hydro-abrosive erosion behaviors of HVOF sprayed Carbide-based Cemet Coatings in Simulated Seawater Slurries, Tribol. lnt, 177, Article (108001).

Jones, M., Horlock, A., Shipway, P., McCartney, D., Wood, J. 2001. A Comparison of the Abrasive Wear Behaviour of HVOF Sprayed Titanium Carbide- and Titanium Boride-Based Cermet Coatings. *Wear*, vol. 251, no. 1–12, pp. 1009–1016. doi:10.1016/S0043-1648(01)00702-5

Kamal, S., Jayaganthan, R., Prakash, S. 2010. Mechanical and Microstructural Characteristics of Detonation Gun Sprayed NiCrAlY+0.4wt% CeO_2 Coatings on Superalloys. *Materials Chemistry and Physics*, vol. 122, no. 1, pp. 262–268. doi:10.1016/j.matchemphys.2010.02.046

Karaoglanli, A.C., Oge, M., Doleker, K.M., Hotamis, M. 2017. Comparison of Tribological Properties of HVOF Sprayed Coatings with Different Composition. *Surfcoat Coatings Technology*, vol. 318, pp. 299–308. doi:10.1016/j.surfcoat.2017.02.021

Karimi, A., Verdon, C., Martin, J.L., Schmid, R.K. 1995. Slurry erosion behaviour of thermally sprayed WC-M Coating. *Wear*, 186-187, pp. 480-486.

Lekatou, A., Zois, D., Grimanelis, D. 2008. Corrosion Properties of HVOF Cermet Coatings with Bond Coats in an Aqueous Chloride Environment. *Thin Solid Films*, vol. 516, no. 16, pp. 5700–5705. doi:10.1016/j.tsf.2007.07.130

Li, C.J., Ohnori, A., Harada, Y. 1996. Effect of Powder Structure on the Structure of Thermaly Sprayed WC-Co Coatings *Journal of Materials and Science*, vol. 31, pp. 785–794.

Lih, W.-C., Yang, S., Su, C., Huang, S., Hsu, I., and M.. Leu, M. 2000. Effects of Process Parameters on Molten Particle Speed and Surface Temperature and the Properties of HVOF CrC/NiCr Coatings. *Surfcoat Coatings Technology*, 133–134, pp. 54–60, doi:10.1016/S0257-8972(00)00873-2

Magnani, M., Suegama, P.H., Recco, A.A.C., Guilemany, J.M., Fugivara, C.S., Benedetti, A.V. 2007. WC-CoCr Coatings Sprayed by High Velocity Oxygen-Fuel (HVOF) Flame on AA7050 Aluminum Alloy: Electrochemical Behavior in 3.5% NaCl Solution. *Materials Research*, vol. 10, no. 4, pp. 377–385, doi:10.1590/S1516-14392007000400010

Magnani, M., Suegama, P.H., Espallargas, N., Dosta, S., Fugivara, C.S., Guilemany, J.M., Benedetti, A.V. 2008. Influence of HVOF Parameters on the Corrosion and Wear Resistance of WC-Co Coatings Sprayed on AA7050 T7. *Surfcoat Coatings Technology,* vol. 202, no. 19, pp. 4746–4757. doi:10.1016/j.surfcoat.2008.04.055

Mahesh, R.A., Jayaganthan, R., Prakash, S. 2008. Oxidation Behavior of HVOF Sprayed Ni–5Al Coatings Deposited on Ni- and Fe-Based Superalloys under Cyclic Condition. *Material Science and Engineering.* A, vol. 475, no. 1–2, p 327–335. doi:10.1016/j.msea.2007.04.108

Murthy, J.K.N., Venkataraman, B. 2006. Abrasive Wear Behaviour of WC–CoCr and Cr3C2–20(NiCr) Deposited by HVOF and Detonation Spray Processes. *Surfcoat Coatings Technology*, vol. 200, no. 8, pp. 2642–2652. doi:10.1016/j.surfcoat.2004.10.136

Myalska, H., Michalska, J.K., Moskal, G., and Szymański, K. 2017. Effect of Nano-Sized TiC Powder on Microstructure and the Corrosion Resistance of WC-Co Thermal Spray Coatings. *Surfcoat Coatings Technology*, vol. 318, pp. 270–278. doi:10.1016/j.surfcoat.2017.01.078

Park, G., Bae, G., Moon, K., and C. Lee, C. 2013. Effect of Plasma Nitriding and Nitrocarburizing on HVOF-Sprayed Stainless Steel Coatings. *Journal of Thermal Spray Technology*, vol. 22, no. 8, pp. 1366–1373. doi:10.1007/s11666-013-0035-4

Pileggi, R., Tului, M., Stocchi, D., Lionetti, S. 2015. Tribo-Corrosion Behaviour of Chromium Carbide Based Coatings Deposited by HVOF. *Surfcoat Coatings Technology*, vol. 268, pp. 247–251. doi:10.1016/j.surfcoat.2014.10.007

Puetz, P., Huang, X., Lima, R.S., Yang,Q., Zhao, L. 2010. Characterization of Transient Oxide Formation on CoNiCrAlY after Heat Treatment in Vacuum and Air. *Surfcoat Coatings Technology*, vol. 205, no. 2, pp. 647–657. doi:10.1016/j.surfcoat.2010.07.079

Sadeghimeresht, E., Markocsan, N., Nylén, P. 2017. Microstructural Characteristics and Corrosion Behavior of HVAF- and HVOF-Sprayed Fe-Based Coatings. *Surfcoat Coatings Technology*, vol. 318, pp. 365–373. doi:10.1016/j.surfcoat.2016.11.088

Sá Brito, V.R.S., Bastos, I.N., Costa, H.R.M. 2012. Corrosion Resistance and Characterization of Metallic Coatings Deposited by Thermal Spray on Carbon Steel. *Matererials and Designs*, vol. 41, pp. 282–288. doi:10.1016/j.matdes.2012.05.008

Sidhu, H.S., Sidhu, B.S., Prakah, S. 2007 , Hot Corrosion Behavior of HVOF Sprayed Coatings on ASTM SA213-T11 Steel. *Journal of Thermal Spray Technology*, vol. 16, no. 3, pp. 349–354. doi:10.1007/s11666-007-9029-4

Sidhu, T.S., Prakash, S. 2006. Hot corrosion and performance of nickel-based coatings. *Current science*, vol. 90, no. 1, pp. 41–47.

Singh, G., Kaur, M., Upadhyaya, R. 2019. Wear and Friction Behavior of NiCrBSi Coatings at Elevated Temperatures. *Journal of Thermal Spray Technology*, vol. 28, no. 5, pp. 1081–1102. doi:10.1007/s11666-019-00876-y

Srinivasan, M., Loganathan, C., Kamaraj, M., Nguyen, Q.B., Gupta, M., Narayanasamy, R. 2012. Sliding Wear Behaviour of AZ31B Magnesium Alloy and Nano-Composite. *Trans. Nonferrous Met. Soc. China (English Ed.*, The Nonferrous Metals Society of China, vol. 22, no. 1, pp. 60–65. doi:10.1016/S1003-6326(11)61140-0

Stokes, J., Looney, L. 2004. Residuol Stress in HVOF Thermally Sprayed thick Deposits. *Surfcoat Coat. Technology*, 177-178, pp. 18–23.

Suarez, M., Bellayer, S., Traisnel, M., Gonzalez, W., Chicot, D., Lesage, J., Puchi-Cabrera, E.S., Staia, M.H. 2008. Corrosion Behavior of Cr3C2–NiCr Vacuum Plasma Sprayed Coatings. *Surfcoat Coatings Technology*, vol. 202, no. 18, pp. 4566–4571. doi:10.1016/j.surfcoat.2008.04.043

Tobergte, D.R., Curtis, S. 2013. Handbook of Thermal Spray Technology. *Journal of Chemical Information and Modeling.*

Torbati-Sarraf, H., Poursaee, A. 2018. Corrosion of Coupled Steels with Different Microstructures in Concrete Environment. *Construction Building Materials*, vol. 167, pp. 680–687.

Verdian, M.M., Raeissi, K., Salehi, M. 2010. Electrochemical Impedance Spectroscopy of HVOF-Sprayed NiTi Intermetallic Coatings Deposited on AISI 1045 Steel. *Journal of Alloys and Compounds*, Elsevier B.V, vol. 507, no. 1, p 42–46. doi:10.1016/j.jallcom.2010.07.132

Verdian, M.M., Raeissi, K., Salehi, M. 2010. Corrosion Performance of HVOF and APS Thermally Sprayed NiTi Intermetallic Coatings in 3.5% NaCl Solution. *Corros Science*, Elsevier Ltd, vol. 52, no. 3, pp. 1052–1059. doi:10.1016/j.corsci.2009.11.034

Verdian, M.M., K. Raeissi, K., Salehi, M. 2012. Characterization and Electrochemical Properties of Ni(Si)/Ni_5Si_2 Multiphase Coatings Prepared by HVOF Spraying. *Applied Surfcoat Science*, vol. 261, pp. 493–498. doi:10.1016/j.apsusc.2012.08.043

Wei, Z.Y., Cui, D.D., Wei, Z., Kory, S. 2023. Effect of Sulphide Concentration on Corrosion Behaviors of HVOF-Sprayed WC-Cr_3C_2-Ni and WC-Ni Coatings. *International Journal of Refractory Metals and Hard Materials*, 111, Article (106104).

Xie, M., Zhang, S., Li, M. 2013. Comparative Investigation on HVOF Sprayed Carbide-Based Coatings. *Applied Surfcoat Science,* vol. 273, pp. 799–805. doi:10.1016/j.apsusc.2013.03.010

Yilbas, B.S., Khalid, M., Abdul-Aleem, B.J. 2003.Corrosion Behavior of HVOF Coated Sheets. *Journal of Thermal Spray Technology*, vol. 12, no. 4, pp. 572–575. doi:10.1361/105996303772082323

Zavareh, M.A., Sarhan, A.A.D.M., Zavareh, P.A., Razak, B.B.A., Basirun, W.J., M.B.C. Ismail, M.C.B. 2016. Development and Protection Evaluation of Two New, Advanced Ceramic Composite Thermal Spray Coatings, Al_2O_3–40TiO_2 and Cr_3C_2–20NiCr on Carbon Steel Petroleum Oil Piping. *Ceramics International vol.* 42, no. 4, pp. 5203–5210, doi:10.1016/j.ceramint.2015.12.044

Zhao, L., Lugscheider, E. 2003. Influence of the Spraying Processes on the Properties of 316L Stainless Steel Coatings. *Surfcoat Coatings Technology*, vol. 162, no. 1, pp. 6–10.

Zhao, W.-M., Wang, Y., Dong, L.-X., Wu, K.-Y., Xue, J. 2005. Corrosion Mechanism of NiCrBSi Coatings Deposited by HVOF. *Surfcoat Coatings Technology*, vol. 190, no. 2–3, pp. 293–298. doi:10.1016/j.surfcoat.2004.04.057

Zmitrowicz, A. 2006. Wear Patterns and Laws of Wear - A Review. *Journal of Theory Applied Mechanics*, vol. 44, no. 1803, pp. 219–253. ◆